HGT

The AAV9 Variant Capsid AAV-F Mediates Widespread Transgene Expression in Nonhuman Primate Spinal Cord After Intrathecal Administration

Adam Beharry,[1] Yi Gong,[2] James C. Kim,[2] Killian S. Hanlon,[2,3] Josette Nammour,[2] Kate Hieber,[1] Florian Eichler,[2,3] Ming Cheng,[2,3] Anat Stemmer-Rachamimov,[3,4] Konstantina M. Stankovic,[5–8] Duane Bradley Welling,[5–7] Carrie Ng,[2] and Casey A. Maguire[2,3,*,i]

[1]*Flagship Biosciences, Inc., Westminster, Colorado, USA;* [2]*Department of Neurology, Massachusetts General Hospital, Charlestown, Massachusetts, USA;* [3]*Harvard Medical School, Boston, Massachusetts, USA;* [4]*Department of Pathology, Massachusetts General Hospital, Boston, Massachusetts, USA;* [5]*Eaton-Peabody Laboratories, Department of Otolaryngology—Head and Neck Surgery, Massachusetts Eye and Ear, Boston, Massachusetts, USA;* [6]*Department of Otolaryngology—Head and Neck Surgery;* [7]*Program in Speech and Hearing Bioscience and Technology; and* [8]*Harvard Program in Therapeutic Science; Harvard Medical School, Boston, Massachusetts, USA.*

[i]*ORCID ID (https://orcid.org/0000-0001-8681-5179).*

Intrathecal delivery of AAV9 into the subarachnoid space has been shown to transduce spinal cord and brain and be less affected by preexisting antibodies, which are lower in cerebral spinal fluid. Still, efficiency of transduction needs to be improved. Recently, we identified a new capsid from a library selection in mice, called AAV-F, that allowed robust transduction of the spinal cord gray matter after lumbar injection. In this study, we test transduction of spinal cord by AAV-F ($n = 3$) compared to AAV9 ($n = 2$), using a reporter gene, in cynomolgus monkeys after lumbar intrathecal injection. Using an automated image analysis (IA) approach to sensitively quantitate reporter gene expression in spinal cord, we found that AAV-F capsid mediated slightly higher transgene expression (both in percentages of cells and intensity of immunostaining) in motor neurons and interneurons, in the lumbar and thoracic regions, compared to AAV9. Interestingly, although AAV-F mediated higher transgene expression in spinal cord, the number of genomes in spinal cord and periphery were on average lower for AAV-F than AAV9, which suggest that lower numbers of genomes were able to mediate higher transgene expression in spinal cord with this capsid. In contrast, dorsal root ganglion transduction efficiency was lower for AAV-F compared to AAV9 on average. Interestingly, we also observed transduction of Schwann cells in sciatic nerve in two nonhuman primates injected with AAV-F, but none with AAV9. Overall, our data demonstrate the utility of automated IA for quantitation of AAV transduction in the spinal cord and the favorable on-target:off-target transduction profile suggests that the AAV-F capsid be considered for gene therapy applications focused on treating the spinal cord after intrathecal delivery.

Keywords: adeno-associated virus, gene delivery, intrathecal delivery, spinal cord, nonhuman primate

INTRODUCTION

AAV VECTOR-MEDIATED GENE THERAPY HAS BECOME an attractive therapeutic option for neuromuscular disorders such as Duchenne muscular dystrophy and spinal muscle atrophy (SMA; clinicaltrials.gov). Delivery to the central nervous system (CNS) to treat genetic disease has advanced to the clinic and AAV9 is U.S. Food and Drug Administration (FDA) approved for systemic injection to treat SMA in infants.[1] Transduction efficiency with AAV9 in the CNS after systemic injection is quite low and other considerations such as dose-limiting toxicity[2,3] and preexisting antibodies[4,5] limit the use of this route of administration for AAV vectors. Intrathecal delivery of AAV9 into the subarachnoid space has been shown to transduce spinal cord and brain and also be less affected by preexisting antibodies, which are lower in cerebral spinal fluid (CSF).[6] Still, there is room for improvement with regard to the efficiency of transduction across different levels of the spinal cord (*i.e.*, lumbar, thoracic, and cervical). Recently, we identified a new capsid from a library selection called AAV-F

*Correspondence: Dr. Casey A. Maguire, Department of Neurology, Massachusetts General Hospital, 149 13th Street, Charlestown, MA 02129, USA. E-mail: cmaguire@mgh.harvard.edu

DOI: 10.1089/hum.2021.069

that showed robust transduction of the spinal cord gray matter after lumbar injection in mice.[7] Here, we test transduction of spinal cord of AAV-F ($n=3$) compared to AAV9 ($n=2$) in cynomolgus monkey after lumbar intrathecal injection. Detecting and quantifying what can be subtle differences across biomarker expression can be challenging.[8] In addition, tissue heterogeneity can pose significant challenges when trying to quantify staining across multiple cell types found within an entire tissue section.[9] Therefore, image analysis (IA) was performed to better determine and quantify the transduction differences found between AAV-F and AAV9. Here, a pathologist-guided cell-based algorithm was trained to identify and quantify the staining of interneurons and motor neurons in each tissue section.

MATERIALS AND METHODS

All methods and experiments were approved by the Partners Institutional Biosafety Committee (IBC) of Partners Healthcare (Massachusetts General Hospital) under IBC approval 2011B000534.

Cell culture

Human 293T cells were obtained from American Type Culture Collection (Manassas, VA). Cells were cultured in high-glucose Dulbecco's modified Eagle's medium (Invitrogen, Carlsbad, CA) supplemented with 10% fetal bovine serum (FBS) (Sigma, St. Louis, MO) and 100 U/mL penicillin and 100 μg/mL streptomycin (Invitrogen) in a humidified atmosphere supplemented with 5% CO_2 at 37°C.

AAV vector production, purification, and titration

For vector production, we used an AAV plasmid driving green fluorescent protein (GFP) as previously described.[10] In brief, the single-stranded (ss) transgene cassette consisted of AAV2 inverted terminal repeats flanking a hybrid cytomegalovirus immediate-early/chicken beta actin promoter (CBA), GFP cDNA, a woodchuck hepatitis virus posttranscriptional regulatory element (WPRE), and SV40 and bovine growth hormone polyA signal sequences.

Production of the AAV9 and AAV-F vectors was done in HEK293T cells. Fifty tissue culture dishes (15 cm diameter) were used (1.5×10^7 cells seeded per plate), with cells cultured in DMEM containing 10% FBS and 100 U/mL of penicillin, 100 μg/mL streptomycin, and 292 μg/mL L-glutamine (Invitrogen). Twenty-four hours after plating, cells were triple transfected using the calcium phosphate method, adding to each plate GFP transgene plasmid (10 μg), rep/cap plasmid (either AAV-F or AAV9, 12 μg), and pAdΔF6 (helper plasmid, 26 μg). Cell media was replaced the day after transfection with DMEM containing 2% FBS. Seventy-two hours posttransfection, AAV was purified from clarified cell lysate by iodixanol density-gradient ultracentrifugation. Buffer exchange to phosphate-buffered saline (PBS) was done using ZEBA spin columns (7K MWCO; Thermo Fisher Scientific) and further concentration was performed using Amicon Ultra 100 kDa MWCO ultrafiltration centrifugal devices (Millipore). We quantified AAV vector genomes (vg) in AAV preparations using TaqMan qPCR with BGH polyA-sequence specific primers and probe.[11] The titer and yield of vectors were as follows: AAV9: Titer, 4.43×10^{12} vg/mL; yield, 6.9×10^{12} vg. AAV-F: Titer, 5.22×10^{12} vg/mL; yield, 1.3×10^{13} vg. Endotoxin for both vector preparations was determined to be <1 EU/mL using Endosafe® LAL Cartridges and the Endosafe nexgen-PTS™ device (Charles River, Charleston, SC). Vector purity was assessed by silver staining of sodium dodecyl-sulfate polyacrylamide gel electrophoresis (SDS PAGE) gels, in which 10^{10} vg of each vector was run/lane. Purity of both preparations were >90%. Vectors were stored at −80°C until use.

Mouse intrathecal bolus injections

All animal experiments were approved by the Massachusetts General Hospital Subcommittee on Research Animal Care following guidelines set forth by the National Institutes of Health Guide for the Care and Use of Laboratory Animals. We used adult age (8–10-week-old) C57BL/6 (strain # 000664) mice from The Jackson Laboratory (Bar Harbor, ME). Mice were put under anesthesia by isoflurane. After the skin over the lumbar region was shaved and cleaned, a 3–4 cm midsagittal incision was made through the skin exposing the muscle and spine. A catheter was inserted between the L4 and L5 spine region and attached to a gas-tight Hamilton syringe with a 33-gauge steel needle. 1×10^{11} vg AAV-F or AAV9 vectors in 10 μL volume were slowly injected at a rate of 5 μL/min. All animals were euthanized three weeks postinjection, perfused transcardially, and tissues were harvested and fixed in 4% formaldehyde in PBS.

Mouse spinal cords and brains immunofluorescence analysis

For imaging of murine whole spinal cord and brain sections, we stained overnight with anti-GFP (cat no. G10362, dilution 1:250; Invitrogen) followed by secondary antibody staining and imaging using a BZ-X800 fluorescence microscope (KEYENCE Itasca, IL).

Nonhuman primate intrathecal injections

Nonhuman primate (NHP) studies were performed at Biomere-Biomedical Research Models (Worcester, MA) according to animal use guidelines and approved procedures. The Test Facility is accredited by the Association for the Assessment and Accreditation of Laboratory Animal Care, International (AAALAC) and registered with the United States Department of Agriculture (USDA) to conduct research in laboratory animals. Five cynomolgus monkeys (*Macaca fascicularis*) were studied (see Table 1 for complete animal information). Animals were consid-

Table 1. *Nonhuman primate study information*

Animal ID	*Age (Years)*	*Weight (kg)*	*Sex*	*Capsid*	*Volume (mL)*	*Dose (vg)*
1001-M529	1.75	1.8	Male	AAV9	0.85	3.76×10^{12}
1102-M444	1.90	1.9	Female	AAV9	0.7	3.1×10^{12}
2101-M452	1.75	1.7	Female	AAV-F	0.85	4.47×10^{12}
2102-M462	1.75	1.8	Female	AAV-F	0.85	4.47×10^{12}
2003-M551	1.75	1.9	Male	AAV-F	0.8	4.17×10^{12}

VG, vector genome.

ered acclimated to the environment at the time of transfer to the study. Before the study, serum from each animal was tested for neutralizing antibodies to AAV9 by the University of Pennsylvania Gene Therapy Program Immunology Core. Titers for all animals were below 1:5.

On Day 0, animals received an IT dose of AAV vector as appropriate to group (Per the study design Table 1). The dose volume injected was 0.7–0.85 mL. There were slight differences in dose between AAV9 and AAV-F owing to two factors. First AAV-F had a slightly higher titer vs. AAV9 (5.22 vs. 4.43×10^{12} vg/mL). Second, we did not have a high enough yield of both capsids to inject the same volume into each animal, which resulted in slightly lower doses in some animals (see Table 1 for exact dosing information). Animals were given Buprenorphine (0.03 mg/kg, IM) and Meloxicam (0.2 mg/kg, SC) before the procedure for the purpose of analgesia. Animals were sedated with Ketamine 7.5–12 mg/kg and Dexdomitor 0.01–0.03 mg/kg mixture, IM; Atipamezole (0.1–0.3 mg/kg, IM) was used for reversal. The animal was positioned in lateral recumbency while on a circulating warm water blanket and/or forced warm air blanket during the procedure. The head was kept in line with the spine and the hips and shoulders were perpendicular to the table. The lower back was arched to increase spacing between the spinous processes. The lumbosacral region (the area over ~L4/5 for cynomolgus) was clipped and aseptically prepared utilizing three alternating scrubs of either povidone iodine or chlorhexidine scrub solution and sponges soaked in 70% isopropyl alcohol. A line block (*i.e.*, Lidocaine/Bupivacaine) approximately 0.20–0.50 mL, SC was administered at the lumbar puncture site. A final application of ChloraPrep™ or appropriate antimicrobial was applied to the puncture site and allowed to dry.

The wings of the ileum were palpated to provide anatomical landmarks. The two spinous processes were identified, and in between which the spinal needle (22 g × 1.5″) was introduced. The skin was penetrated and needle slowly advanced. After confirmation of placement in the intrathecal space, ~0.5 mL of CSF was removed before dose administration. Next, the AAV vector was slowly administered over 1–2 min. After administering the dose, the syringe and needle was left in place for ~5 s and after removal, pressure applied to the injection site. Parameters were observed constantly throughout the procedure, including heart rate, respiratory rate, and oxygen saturation. Animals were recovered from anesthesia and moved to a recovery area, placed on a circulating warm water blanket and/or forced warm air blanket and covered with a dry towel. Animals were observed following the procedure and kept in the recovery area until the animal was conscious able to hold itself in a sitting position. Animals were then transported to their home cage. Approximately 2 h post vector dosing, animals were immunosuppressed with intramuscular dosing of 0.5 mg/kg of dexamethasone, which continued daily until necropsy at day 21.

NHP Necropsy and tissue processing

On Day 21 ± 1 day, animals were anesthetized with Ketamine 7.5–12 mg/kg and Dexdomitor 0.01–0.03 mg/kg mixture. Nembutal was administered at 15–30 mg/kg. Once deeply anesthetized, the animal was perfused via left cardiac ventricle with cold heparinized (100 U/mL) saline until the outflow ran clear. Approximately 1 L of heparinized saline was used with a perfusion pump set to ~400 rpm. Euthanasia was performed per American Veterinary Medical Association (AVMA) guidelines. Samples for paraffin embedding were fixed in 10% neutral buffered formalin before transferring the samples to PBS. Samples for cryosectioning were fixed in 4% buffered formaldehyde for 24 h before transferring samples to PBS. Samples for qPCR analysis were collected using a 4 mm biopsy punch and immediately frozen on dry ice and stored at −80°C.

NHP histology performed at Flagship Biosciences

Four micrometer thick formalin-fixed paraffin-embedded tissue blocks were prepared for each section stained with GFP. All staining was performed on a Ventana Discovery Ultra automated staining system (Roche Diagnostics, Germany) using Ventana reagents according to the manufacturer's instructions. All slides were treated with standard cell conditioning solution CC1 with a GFP antibody (ab6556, Abcam) concentration of 5 μg/mL. Slides were then digitized utilizing Aperio's CS bright-field scanning system (Leica Biosystems, Buffalo Grove, IL) at Flagship Biosciences' tissue analysis laboratory (Westminster, CO). To ensure optimal scanning, at least four focal points were set for each slide and acquired at 20× scanner settings. All whole-slides images were assessed for blurring or ''stitching'' artifacts and rescanned until passing Flagship's quality-assessment for digital scans.

IA performed at Flagship Biosciences

All personnel, including the pathologist, were blinded to the identity of vector for all samples. Only the animal ID was provided to Flagship Biosciences. A minimum of 10 whole-slide scanned digital images were generated for each animal. Any digital image not containing the tissue of interest was excluded from analysis resulting in a total of 40 images analyzed. A minimum of 604 of either motor or interneurons were identified and analyzed per animal. Each whole-slide scan digital image was analyzed using Flagship Bioscience's proprietary computational Tissue Analysis, cTA™, (Westminster, CO). Regions of interest were established around the target tissue (gray matter), while also excluding staining and tissue artifacts (*i.e.*, tissue folds, artifacts, mounting media, and so on). To differentiate neuronal populations, the algorithm used hematoxylin staining to identify nuclei and 3,3′-diaminobenzidine (DAB) staining to identify morphological and staining cell features. Implementing a decision tree strategy, interneuron and motor neuron training regions were manually identified to assist the algorithm. A minimum of two training regions per sample were used and increased if there was a misclassification of neurons upon review. These training regions provided the algorithm cellular features (membrane and nuclear) used to segregate interneurons and motor neurons from the entirety of a sample's cell population. Each individual sample only used the training regions from that specific sample to account for any subtle differences in morphology and staining that may exist. GFP staining intensity for each nucleus-identified interneuron or motor neuron was quantified based on the mean staining density (MSD) of DAB staining. The methodology used to detect and quantify cellular staining has been previously described.[8,12] The DAB MSD from tissue not transduced with a GFP-expressing vector was used to determine the appropriate positive or negative threshold. All activities were assessed by a board-certified pathologist to verify the algorithm performance and accuracy.

NHP spinal cord immunofluorescence analysis

NHP spinal cord tissue as well as attached dorsal root ganglion (DRG) from different levels were fixed in 4% formaldehyde in PBS and then balanced in 30% sucrose. Tissues were further embedded and then sectioned at 12 μm thickness in a cryostat. Tissue sections were costained with GFP and one of the four cellular markers: neurofilament (NF) for neurons, glial fibrillary acidic protein (GFAP) for astrocytes, IBA1 for microglia, and Olig2 for oligodendrocytes at 4°C for 24 h. Primary and secondary antibody combinations were listed in the table below. Sectioned were then imaged by fluorescence microscope (Zeiss).

Costaining Group	*Primary Antibodies*	*Secondary Antibodies*
GFP+NF	GFP: Invitrogen G10362 1:300 NF: BioLegend SMI-32 1:1,000	Alexa fluor 488 goat anti-rabbit 1:1,000 Alexa fluor 555 goat anti-mouse 1:1,000
GFP+GFAP	GFP: Abcam ab1218 1:1,000 GFAP: Dako Z0334 1:500	Alexa fluor 488 goat anti-mouse 1:1,000 Cy™3 donkey anti-rabbit 1:600
GFP+IBA1	GFP: Abcam ab1218 1:1,000 IBA1: Wako 019–19741 1:500	Alexa fluor 488 goat anti-mouse 1:1,000 Cy™3 donkey anti-rabbit 1:600
GFP+Olig2	GFP: Abcam ab1218 1:1,000 Olig2: Millipore AB9610 1:500	Alexa fluor 488 goat anti-mouse 1:1,000 Cy™3 donkey anti-rabbit 1:600

Quantitation of AAV genomes in spinal cord and peripheral tissues

DNA was isolated from fresh-frozen tissue punches using the DNeasy blood and tissue kit (Qiagen). DNA was quantitated using a NanoDrop spectrophotometer (ThermoFisher Scientific). A qPCR was performed to detect AAV genomes in the isolated DNA using the same TaqMan probe and primer set as described above in AAV vector production, purification, and titration. For each sample, an equal input of DNA was used for the qPCR. A separate qPCR reaction for each sample was performed to detect the NHP gene UBE2D2 (ubiquitin conjugating enzyme E2 D2) using the TaqMan Gene Expression Assays 20x mix (cat. no. 4351372, assay ID Mf07285893_s1; ThermoFisher Scientific) to normalize for equal loading. AAV genomes were inferred from the AAV plasmid standard curve and adjusted to AAV genomes/μg of genomic DNA. Values were normalized to the lowest Ct value of the UBE2D2 qPCR to ensure equal DNA input. All qPCR was performed in a 7500 FAST qPCR system (Applied Biosystems).

Statistical analyses

Due to the small number of nonhuman primates used in this study, and the high variability observed in outbred animals, we did not feel it appropriate to provide statistical analyses for the different comparisons. We therefore considered this study an exploratory study and comparisons are qualitative, and we refer to differences between groups as ''trends.''

RESULTS

Intrathecal bolus injection of AAV-F in mice results in robust transduction of gray matter in the spinal cord of mice

We have previously reported that AAV-F leads to high levels of transgene (GFP) expression in the spinal cord of mice injected via the bolus lumbar route.[7] Before performing the intrathecal injections in NHPs, we first validated the purity of the AAV9 and AAV-F vectors by silver

stain. Purity of both vector preparations was at least 90% (Supplementary Fig. S1). Interestingly, we noticed a lower than expected VP2 ratio compared to VP1 (it is expected to be 1:1). The reason behind the lower ratio is unknown at this time, but was consistent for both capsids. A recent report suggests heterogeneity of this ratio, even within the same preparation of vector.[13] Next, we tested the potency of each vector preparation by performing bolus lumbar intrathecal injections of adult mice. Mice were injected with 10^{11} vg each ($n=2$ mice/vector) of AAV9-CBA-GFP or AAV-F-CBA-GFP. Three weeks later, mice were killed and cryosections of spinal cord were immunostained for GFP detection with fluorescently labeled secondary antibodies. As we previously reported,[7] we observed robust expression of GFP in the gray matter with AAV-F compared to AAV9, which was mainly restricted to the white matter (Fig. 1 and Supplementary Fig. S2). Also, we observed efficient transduction of the brain with AAV-F compared with AAV9 (Supplementary Fig. S3).

Immunofluorescence analysis of NHP spinal cord transduction by AAV-F and AAV9 after intrathecal injection

Cynomolgus monkeys were injected intrathecally (lumbar region) with AAV9-CBA-GFP ($n=2$) and AAV-F-CBA-GFP ($n=3$; Table 1). Nearly identical amounts of vector were injected into each animal (range 3.1–4.47×10^{12} vg). All injections were tolerated well, and no notable events occurred during the study regarding any of the animals' behavior or health. Animals were killed three weeks postinjection, and spinal cords cut in 1 cm cross sections to allow assessment of GFP expression in cervical, thoracic, and lumbar/sacral regions. We costained cryosections with an anti-GFP antibody and one of four markers for neurons (NF), astrocytes (GFAP), microglia (IbaI), and oligodendrocytes (olig2) and analyzed sections by confocal microscopy. For both AAV9 and AAV-F, GFP-positive neurons were readily detected (Fig. 2) with some variance in efficiency between each animal. GFP-positive astrocytes were detected for both capsids, but less frequently than for neurons (Fig. 2). Rare GFP-positive microglia and oligodendrocytes were detected for both capsids (Fig. 2).

In AAV-F-injected animals 2003 (male) and 2102 (female), we observed intense GFP immunofluorescence at the cervical level in the dorsal column of the spinal cord, which appeared to be GFP-filled axons as revealed by costaining with NF (Supplementary Fig. S4). We also observed GFP immunostaining in DRG neurons as well as along the nerve (Supplementary Fig. S5).

Automated IA of cell type quantitation of transduction of spinal cord by AAV-F and AAV9 in NHP after intrathecal injection

To perform a quantitative analysis of spinal cord transduction with a higher sensitivity than immunofluorescence analysis, immunohistochemical staining using horseradish peroxidase-mediated signal amplification and DAB development of spinal cord and DRG for GFP was performed. As expected, transduction of DRG neurons at all levels of the spinal cord was observed for both capsids, with the lumbar region giving the highest staining

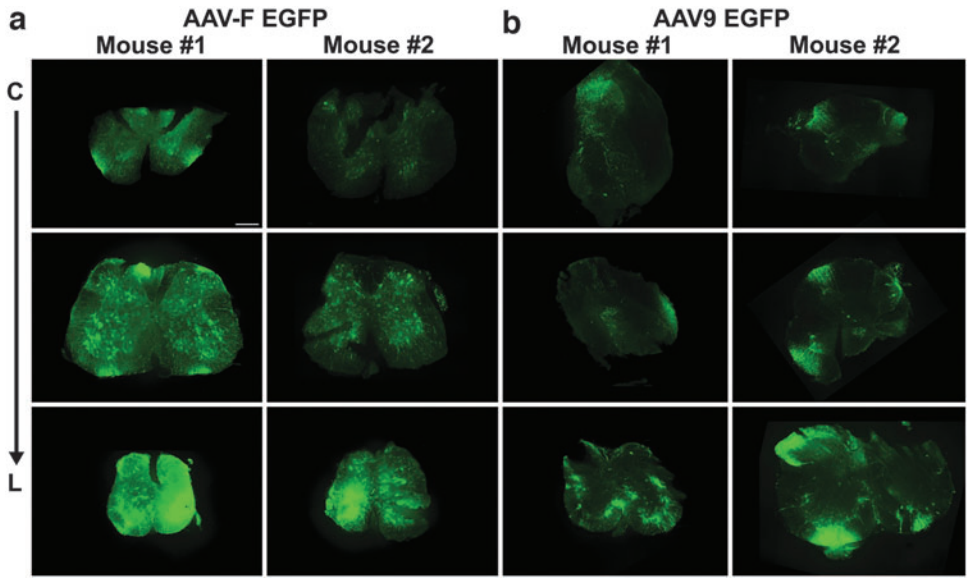

Figure 1. AAV-F robustly transduces the *gray* matter of spinal cord after intrathecal injection in adult mice. Adult mice were injected via the lumbar region with AAV9 or AAV-F encoding GFP at a dose of 1×10^{11} vg ($n=2$/vector). Panels depict spinal cord sections immunostained for GFP expression of mice injected with **(a)** AAV-F and **(b)** AAV9. For each animal, *top* to *bottom* is cervical, thoracic, and lumbar regions of the spinal cord. GFP, green fluorescent protein; vg, vector genome.

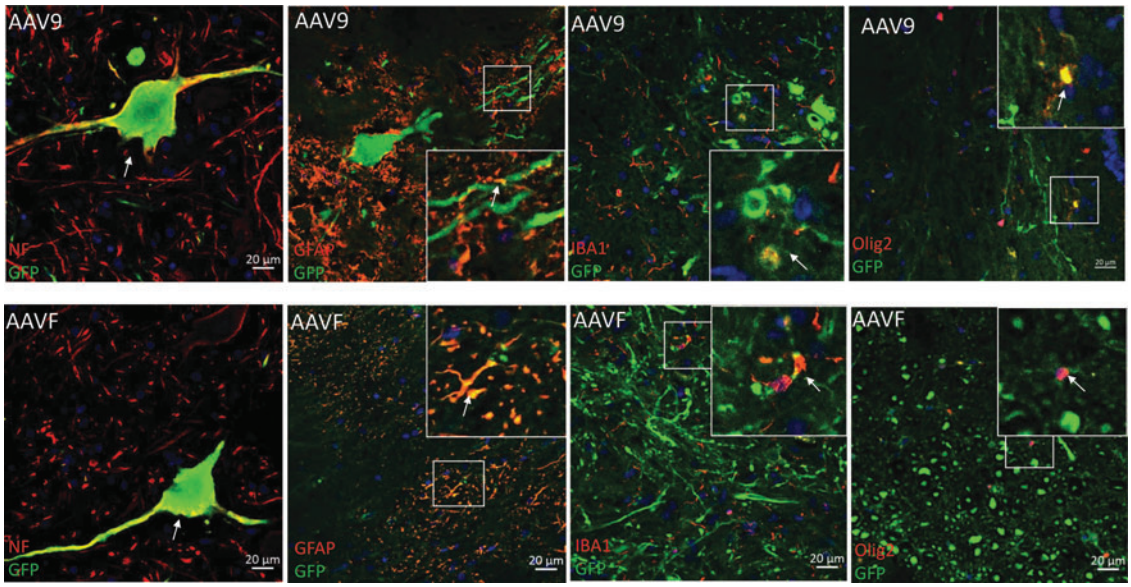

Figure 2. Cell type transduction in spinal cord tissue of NHPs by intrathecal delivery of AAV9-GFP and AAVF-GFP. Tissue sections were costained for GFP with different cellular markers: NF for neuron, GFAP for astrocyte, IBA1 for microglia, olig2 for oligodendrocytes. Scale bar = 20 μm. *White arrows* indicate costaining. GFAP, glial fibrillary acidic protein; NF, neurofilament; NHPs, nonhuman primates.

intensity (Fig. 3a). In the lumbar region, some of the intensely GFP-labeled neurons had an abnormal morphology, likely due to transgene toxicity, which has been recently described by the Wilson group.[14] Quantitation was performed using a proprietary IA software system. The software was trained by a board-certified pathologist to morphologically distinguish GFP-immunoreactive DRG neurons in NHPs injected with AAV-F or AAV9. There were not enough cervical sections with DRG, so we analyzed only thoracic and lumbar regions. Interestingly in both thoracic and lumbar regions, AAV9 transduced a higher percentage of DRG neurons, 1.6- and 2-fold, respectively, compared to AAV-F (Fig. 3b). We also used the IA software to quantitate staining intensity of GFP-positive DRG in the thoracic and lumbar regions for both vectors. There was a small enhancement in the mean staining intensity in the AAV-F-injected group in both spinal cord regions compared to AAV9 (Fig. 3c). To minimize any staining variability, all sections were cut the same section thickness and processed on an autostainer using the same lot of antibody. However, it cannot be ruled out that preanalytical variables may have contributed to some of the differences in GFP expression observed.

In the spinal cord, GFP expression was readily detected in motor neurons in the ventral horns with both capsids in all injected animals, and at all levels of the spinal cord (Fig. 4a and Supplementary Fig. S6). As in the immunofluorescence analysis, we noticed intense GFP immunoreactivity in the dorsal column in DAB sections in animals 2102 and 2003 injected with AAV-F (Fig. 4b).

The IA software was trained by a board-certified pathologist to morphologically distinguish GFP-immunoreactive motor neurons and interneurons (Supplementary Fig. S7). Next, we quantitated both the percentage and staining intensity of transduced motor neurons and interneurons for both capsids in the lumbar, thoracic, and cervical regions of the spinal cord. A gradient of transduction from lumbar (higher) to cervical (lower) was observed in motor neurons for both capsids, (range of 39.18% to 69.61% GFP-positive cells, Fig. 5a). A gradient was also observed for interneurons with the exception of a lower percentage of interneurons in thoracic region vs cervical region for AAV9 (range of 16.05% to 56.25% positive cells Fig. 5a). Comparison of the percentages of interneurons and motor neurons between AAV9 and AAV-F in the entire spinal cord revealed an increase with AAV-F (Fig. 5b). Regional comparison of interneuron transduction revealed that AAV9 mediated slightly higher percentages of cells in the cervical region, while AAV-F had higher percentages in the thoracic and lumbar regions (Fig. 5c). For motor neurons, AAV-F mediated slightly higher transduction efficiencies in all three regions of the spinal cord compared to AAV9 (Fig. 5d). The sensitivity of the automated IA also allowed us to quantitate the staining intensity in GFP immunoreactive cells, which indicates levels of transgene product/cell. AAV-F mediated a 12.9% and 11.2% higher level of staining intensity in motor and interneurons, respectively, compared to AAV9 when analyzed for the entire spinal cord (Fig. 5e). For regional analysis, AAV-F mediated a slight, yet, detectably higher staining intensity in both thoracic and lumbar regions for both cell types (Fig. 5f). The data were also presented in individual animal format for both % transduction and mean GFP staining intensity (Supplementary Fig. S8). For AAV9, animal

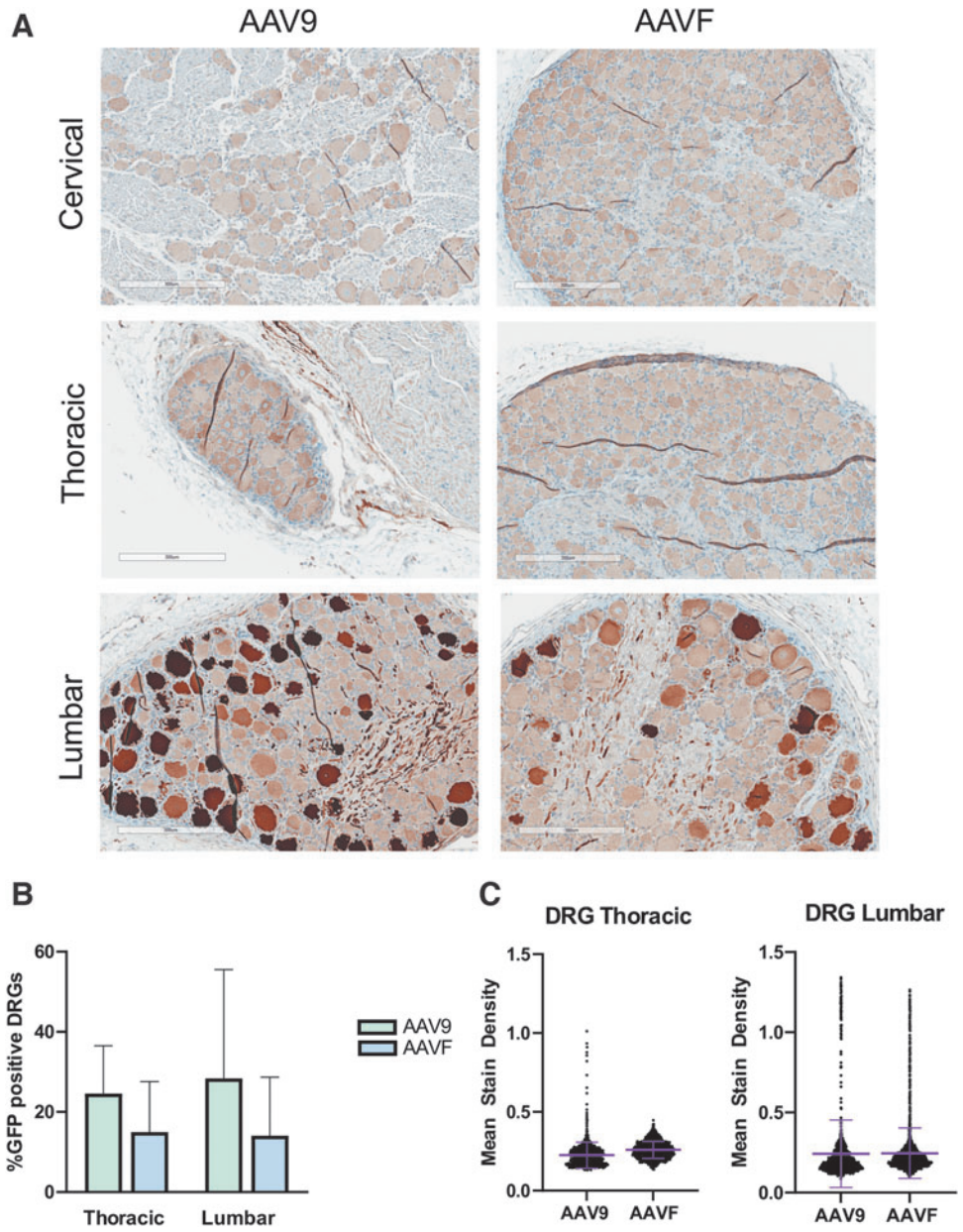

Figure 3. AAV9 and AAV-F robustly transduce DRG neurons after intrathecal delivery to NHPs. **(a)** Anti-GFP immunohistochemistry was performed on DRG sections at three levels of the spinal cord. DAB *brown* staining indicates specific GFP detection. Scale bars = 300 μm. **(b)** Percentage of DRG positive for GFP in thoracic and lumbar regions. **(c)** Mean staining intensity of transduced DRG in thoracic and lumbar regions. Mean ± standard deviation are shown. Individual cells are shown as *black* data points. DAB, 3,3′-diaminobenzidine; DRG, dorsal root ganglion.

1001 (male) had a higher transduction efficiency in the lumbar region with lower efficiency in cervical and thoracic regions. In contrast animal 1102 (female), efficiency was more consistent throughout the spinal cord for both neuronal types. For AAV-F, animal 2003 (male) had the highest transduction efficiency and staining intensity across the spinal cord compared to the two female animals, although there was a lot of variability between regions/animals.

Immunohistochemical analysis of transduction of AAV-F and AAV9 in NHP brain after intrathecal injection

While the primary goal of this study was to evaluate the transduction efficiency of the spinal cord by AAV-F and AAV9, we also qualitatively assessed brain transduction in immunohistochemically stained sections. For both capsids, we observed transduced cells in cerebellum, brain stem, and hippocampus (Fig. 6).

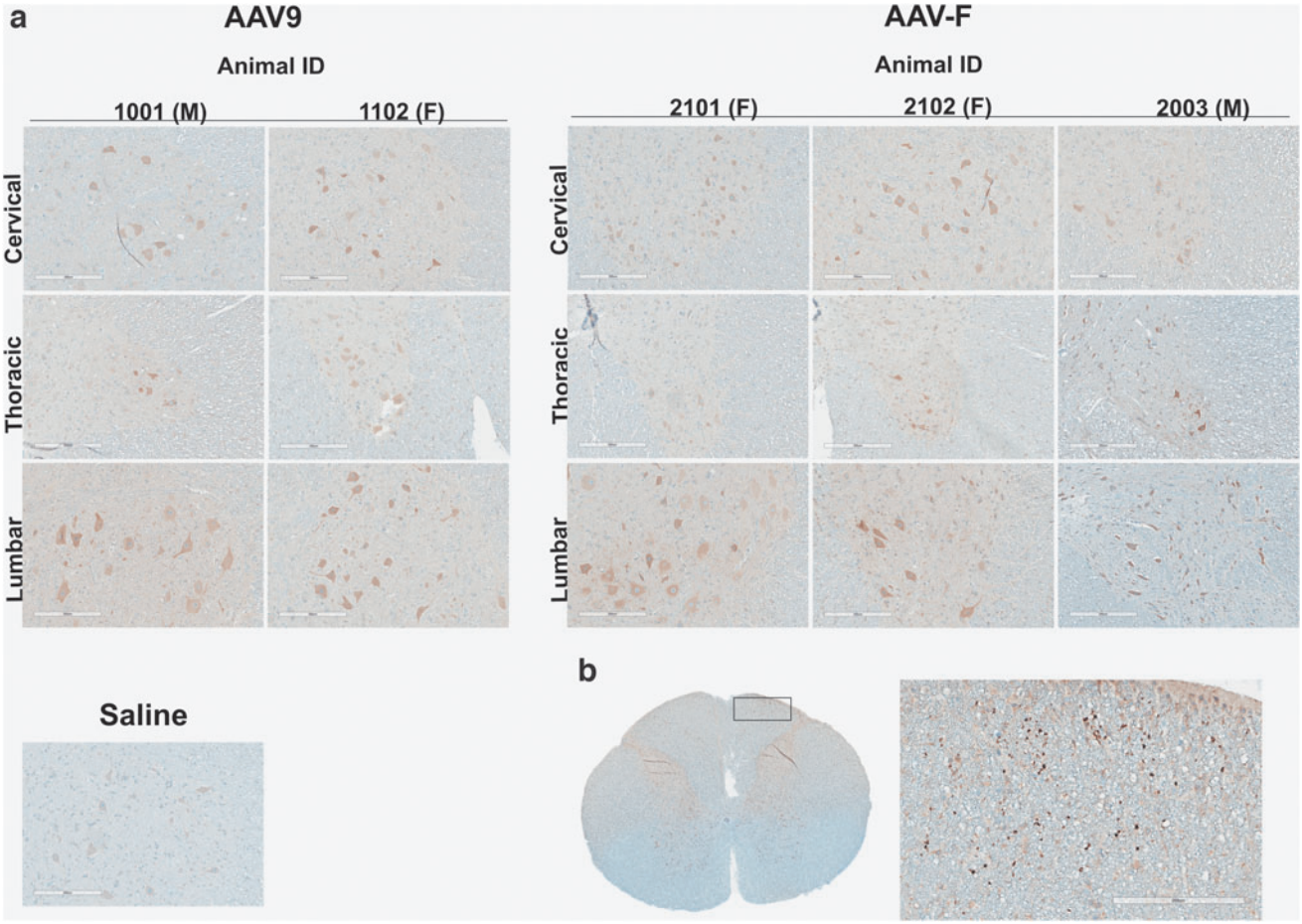

Figure 4. AAV9 and AAV-F transduce neurons in the ventral horn of the spinal cord after intrathecal delivery to NHPs. **(a)** Representative images depicting anti-GFP immunohistochemistry shown at three levels of the spinal cord for all NHPs injected with AAV9 ($n=2$) or AAV-F ($n=3$) in the study. DAB *brown* staining indicates specific GFP detection. Animal IDs are indicated as well as animal sex (male, M; female, F). The saline image is from an animal injected with vehicle to show background staining. Scale bars = 300 μm. **(b)** Robust GFP immunoreactivity was detected in the spinal column of 2/3 NHPs injected with AAV-F. Representative image is shown with *low* magnification image depicting the area of the spinal cord the *high* magnification image is derived from. Scale bar = 200 μm.

Biodistribution and transduction analysis of AAV9 and AAV-F in spinal cord and peripheral organs

In addition to the transgene expression data, we measured AAV genomes in spinal cord (cervical, thoracic, and lumbar regions) as well as liver, spleen, and heart. In spinal cord, the mean amount of AAV genomes was higher for AAV9 compared to AAV-F at all three levels, ranging from 1.83- to 6.3-fold, (Fig. 7a). The mean for AAV9 genomes was also higher than AAV-F in liver (4.87-fold higher), spleen (3.85-fold higher), and heart (2.17-fold higher) (Fig. 7b). Genomes in the brain were low to undetectable for most samples (data not shown).

We also analyzed the qPCR data separately for each animal (Fig. 7c–g). From this plot of the data, it was clear that vector genomes were quite variable across the spinal cord between animals, especially those injected with AAV-F. We noticed that one of the AAV9-injected animals (id# 1102, female) and one of the AAV-F-injected animals (id #2003, male) had more even distribution of vector genomes across the spinal cord and a higher spinal cord/liver genome copy ratio, perhaps indicating less leakage of vector to the periphery with these particular injections. Interestingly, animal 2003 was the animal with highest transduction efficiency in spinal cord (Supplementary Fig. S8).

Since we observed an across-tissue/organ lower genome amount for AAV-F compared to AAV9, we wanted to ensure this was not due to an inadvertent lower dosing due to vector binding to the syringe or needle used to inject the NHPs. Subsequently, we performed a biocompatibility analysis of each capsid with the same syringe/needle used in the NHP injections. No loss of either capsid was observed, suggesting that the intended dose of each vector was injected into NHPs (data not shown).

To assess whether the transgene expression by each vector matched the biodistribution data, we performed immunofluorescent detection of GFP expression in liver

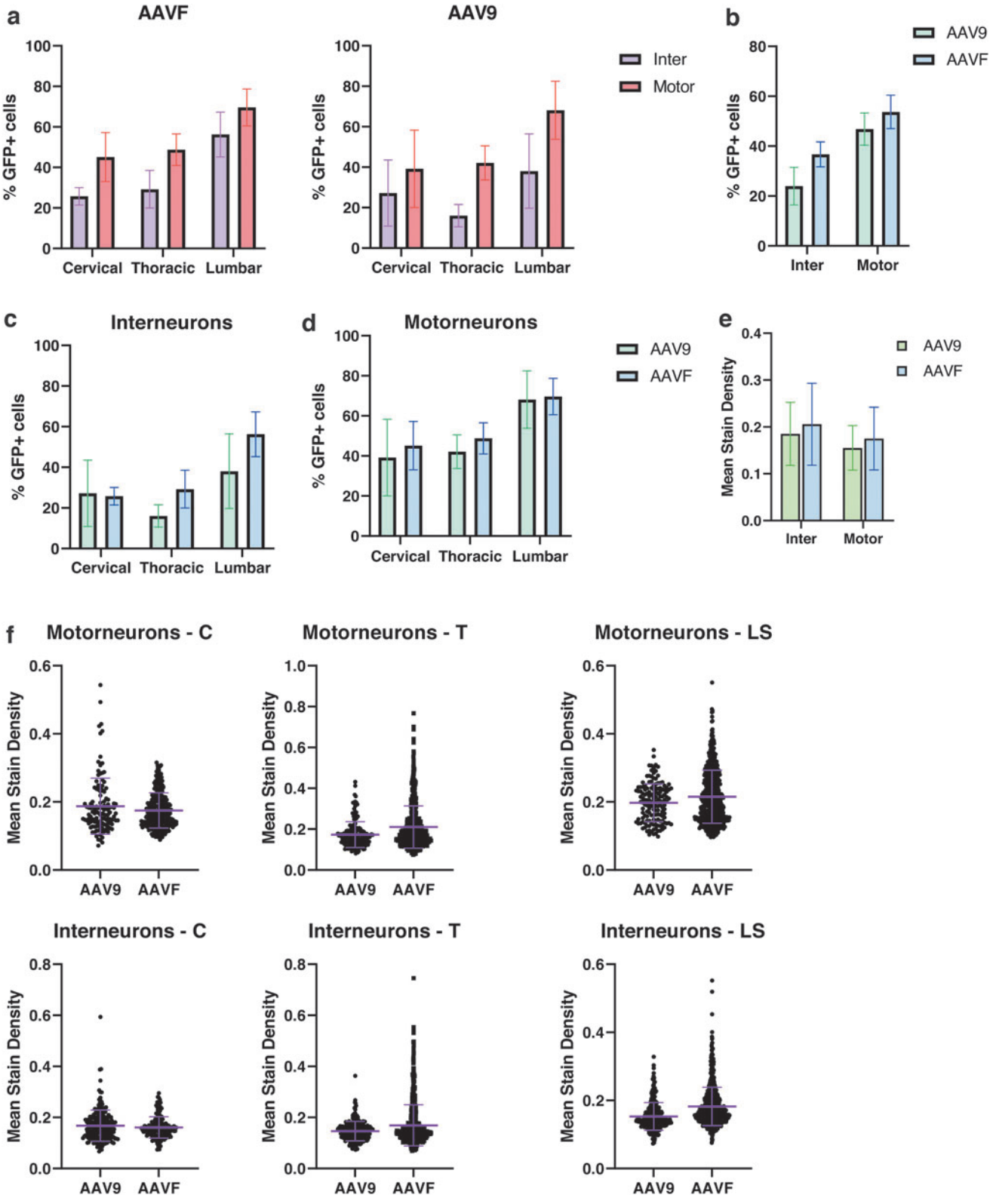

Figure 5. Automated image analysis of spinal cord transduction. **(a)** Transduction efficiency in percentages of GFP immunopositive motor neurons and interneurons for AAV-F (*left*) and AAV9 (*right*) across cervical, thoracic, and lumbar regions. Comparison of transduction efficiency in % positive cells between AAV9 and AAV-F **(b)** across the entire spinal cord, **(c)** in spinal cord regions for interneurons, and **(d)** spinal cord levels for motor neurons. Comparison of transduction levels/cell (mean stain intensity) between AAV9 and AAV-F **(e)** across entire spinal cord and **(f)** regions of spinal cord. Mean ± standard deviation are shown. Individual cells are shown as *black* data points. C, cervical; T, thoracic; LS, lumbar-sacral.

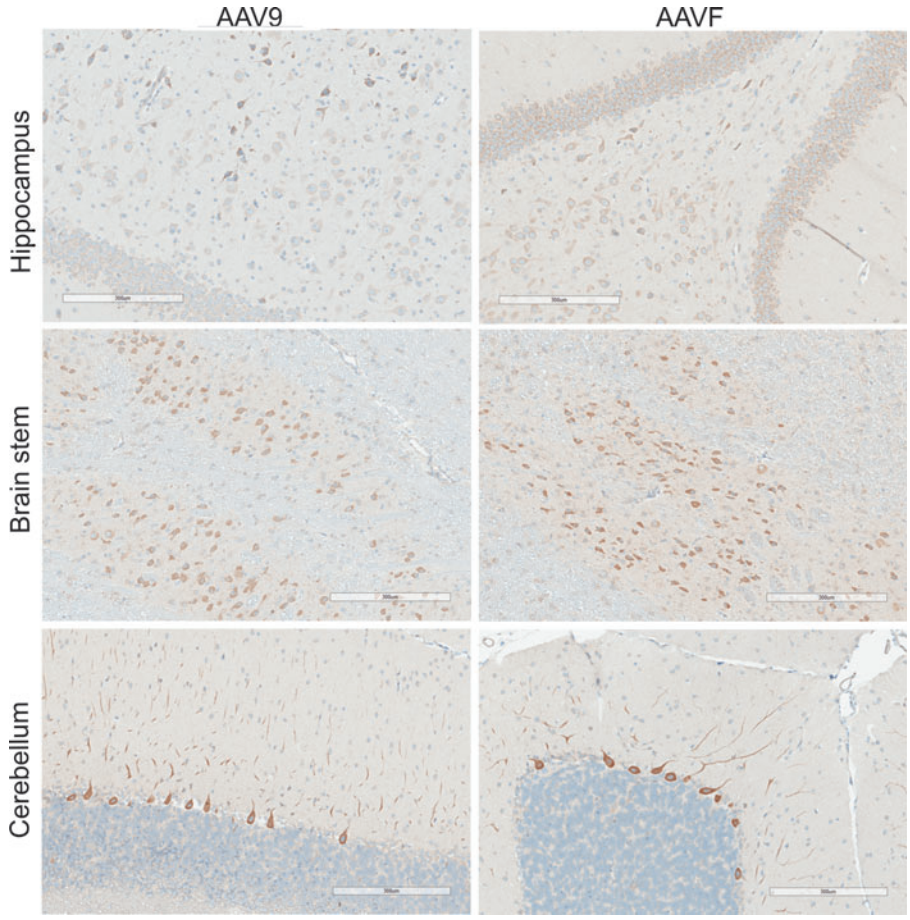

Figure 6. Brain transduction by AAV9 and AAV-F. Representative images depicting anti-GFP immunohistochemistry shown at three regions in the brain for NHPs injected with AAV9 or AAV-F. Scale bars = 300 μm. DAB *brown* staining indicates specific GFP detection.

and heart cryosections for all animals. In liver, AAV9 transduced a high percentage of hepatocytes in animal 1001 (male), while not detectably transducing cells in animal 1102 (female) (Supplementary Fig. S9). This result tracked with the qPCR data, in which AAV9 had higher levels of genomes in liver for animal 1001 (male) versus 1102 (female) (Fig. 7). For AAV-F, all three animals had detectable GFP expression, which was observed as low percentages of GFP+ cells, but intermittent very bright immunofluorescent labeled single cells (Supplementary Fig. S9). The male animal 2003 seemed to have more cells transduced than the female animals in this group, but it was still lower than the male NHP injected with AAV9. In heart, for all animals and both vectors, very sparse transduction was observed, although AAV-F transduced cells were much brighter (Supplementary Fig. S10).

AAV-F transduces peripheral nerves

We harvested sciatic nerve from all AAV9- and AAV-F-injected animals. Nerves were sectioned and immunostained for GFP in serial sections. No GFP immunoreactive cells were observed for either animal injected with AAV9-CBA-GFP. In contrast, we observed sparse, yet, specific GFP immunostaining in two out of three NHPs (animals #2101 and #2102, both females) injected with AAV-F-CBA-GFP (Fig. 8 and Supplementary Fig. S11). Many of the GFP^+ cells had elongated nuclei and were randomly distributed; the morphology and distribution was consistent with Schwann cells. Some immunostaining was observed in endothelial cells lining small capillaries, both in the nerve and also in the adjacent fat.

DISCUSSION

This study evaluated the transduction efficiency of a recently described AAV9 capsid variant, AAV-F, after intrathecal injection of NHPs. Using automated imaging analysis, we quantitated transduction efficiency of interneurons and motor neurons. Overall, we found a slightly higher transduction efficiency using AAV-F compared to AAV9 with the same transgene expression cassette (AAV-CBA-GFP). However, it is important to recognize that this was a small study due to the expense of NHP research as well as ethical concerns ($n = 2$ for AAV9 and $n = 3$ for AAV-F). Therefore, we view these findings as laying the

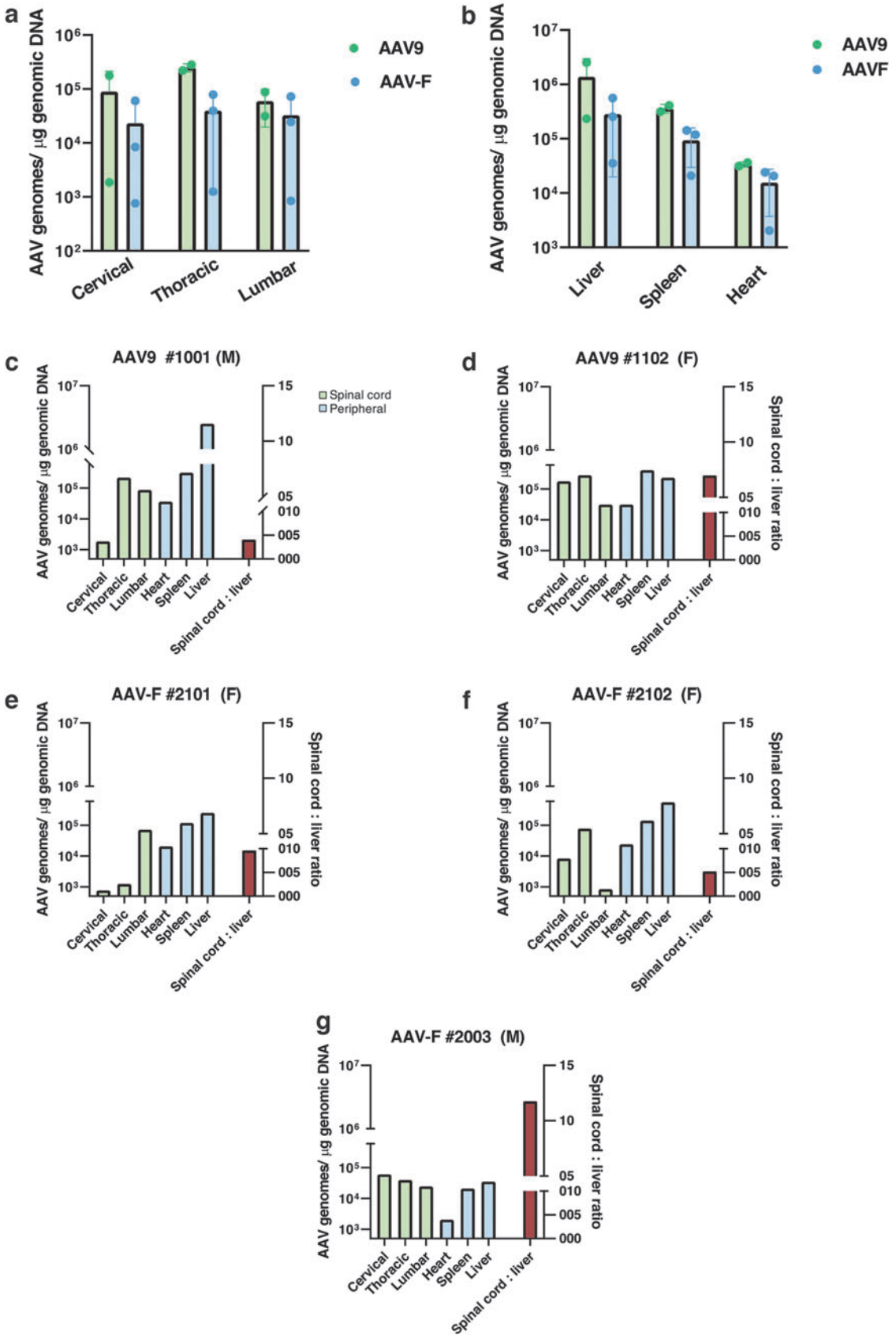

Figure 7. Biodistribution of AAV9 and AAV-F in spinal cord and peripheral organs. Tissues were harvested 3 weeks postintrathecal injection and DNA isolated. qPCR was performed to detect AAV genomes as well as the NHP gene UBE2D2 to ensure equal input/sample. **(a)** AAV genomes/μg genomic DNA in cervical, thoracic, and lumbar regions of the spinal cord. **(b)** AAV genomes/μg genomic DNA in liver, spleen, and heart tissue. Error bars represent SEM and individual data points represent individual animals. **(c–g)** Individual animal biodistribution data. *Right* axis denotes spinal cord to liver ratio (colored in *brown*). SEM, standard error of the mean.

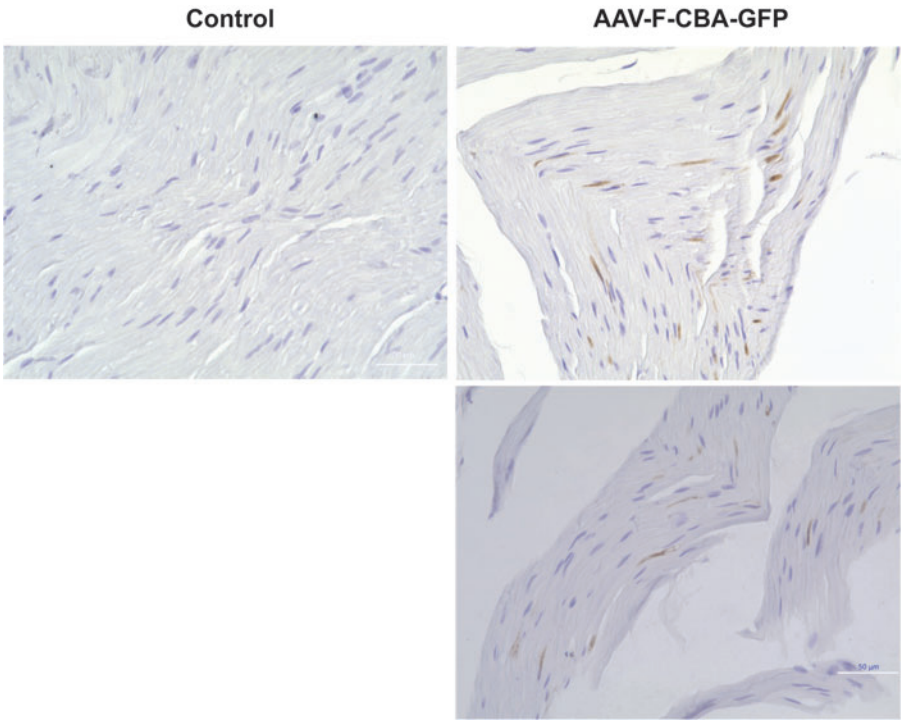

Figure 8. AAV-F, but not AAV9, detectably transduces peripheral sciatic nerve cells after intrathecal injection. DAB *brown* staining indicates specific GFP detection.

groundwork for further studies with this capsid in larger numbers of animals to evaluate the full potential of the capsid for transgene efficiency in the spinal cord. In this study, a relatively low dose for each vector was injected (range $3.1–4.47\times10^{12}$ vg/animal), which was limited by our laboratory's relatively small-scale production size (we produce vector in adherent 293T in tissue culture dishes). The dose was particularly low considering that the transgene cassette was in a single-stranded genome of AAV. Most studies in the NHP CNS have been performed with the higher efficiency self-complementary genome (see below). We chose to use a single-stranded genome to evaluate the capsid's performance in a manner that would be relevant to all transgenes that fit into AAV's ~5 kb packaging capacity. Despite the dose being relatively low with a single-stranded AAV9 vector, we observed transduction efficiency of motor neurons from 68.1% in lumbar, 42.1% thoracic, and 39.2% in cervical region. Meyer *et al.* used intrathecally injected self-complementary AAV9-GFP in NHPs at 1×10^{13} vg/kg and found that $\sim$70% (lumbar), 50% (thoracic), and 30% (cervical) motor neurons were GFP positive.[15] Gray *et al.* used self-complementary AAV9-GFP at an intrathecal dose of 2×10^{12} vg and 5×10^{12} vg.[6] They observed 66% (lumbar), 41% (thoracic), and 43% (cervical) positive cells per NHP. Bey *et al.* utilized a self-complementary AAV9-GFP vector injected intrathecally in NHPs at a dose of 2.5×10^{13} vg.[16] Transduction efficiency of motor neurons was reported to be up to 66% (lumbar), 59% (thoracic), and 45% (cervical). While one must be cautious when comparing studies due to a variety of variables, including AAV titration differences, differences between genomes (single-stranded vs self-complementary), and promoter and other elements, the transduction efficiencies in spinal cord with a single-stranded AAV9 vector in our study are relatively close to that obtained in the other studies using self-complementary AAV9 vectors. This bodes well for intrathecal strategies, which require the full packaging capacity and therefore a single-stranded AAV genome. In future studies, a wider dose range, from $\sim3\times10^{12}$ vg to 3×10^{13} vg, could be evaluated, as well as testing whether packaging a self-complementary genome increases transduction efficiency.

Comparisons of tropism and efficiency of transduction between AAV9 and AAV-F could readily be made given both vectors were produced, purified, and titered by the same laboratory. Due to slight differences in titer and yield, animals received slightly higher doses of AAV-F (19–44% higher). This could be interpreted as a potential bias toward the AAV-F vector, although we find this unlikely to have affected the overall conclusions. First as AAV-F had less vector genomes on average in the spinal cord and peripheral organs, but as good or higher transgene expression as AAV9 in spinal cord, our conclusion that AAV-F actually has higher potency in spinal cord than AAV9, likely stands. Also, we observed that AAV9 trended toward higher percentages of transduced DRG than AAV-F, so it appears that there are bona-fide transduction differences with the two

capsids. Further, Schwann cells transduction was only detected with AAV-F and none with AAV9 and the small dose difference is unlikely to explain this outcome.

One interesting observation of our study was that while AAV-F mediated slightly higher or better transduction of spinal cord compared to AAV9, it displayed a lower amount of vector genomes in the spinal cord compared to AAV9. This observation indicates that the transduction increase in certain area of the spinal cord (*i.e.*, lumbar, thoracic regions) with AAV-F was not simply due to better biodistribution to these cells compared to AAV9, in fact, it would appear from these data that physical biodistribution under the tested conditions is less efficient with AAV-F. One explanation for this finding is that despite having fewer genomes in the spinal cord, more genomes may have been uncoated for AAV-F compared to AAV9, leading to better expression at three weeks postinjection. Uncoating kinetics has been proposed as a mechanism for enhanced transduction of AAV8 over AAV2 *in vivo*.[17] Our method of isolation and qPCR for the biodistribution did not distinguish between uncoated and encapsidated genomes. In the future, if AAV-F is explored further for CNS mediate transgene expression in NHPs, a time course of expression compared to AAV9 would be important to understand transgene expression kinetics. If AAV-F is indeed more potent than AAV9 on a per-genome basis, increasing its biodistribution throughout the spinal cord by placing animals in the Trendelenburg position[15,18]; it may allow better transduction of the cervical region of the spinal cord compared to AAV9. It may also be worthwhile to inject AAV-F directly into the lateral ventricles to enhance brain transduction.

One notable finding of our study was the difference in brain transduction by AAV-F in mice compared to NHPs. In mice AAV-F mediated enhanced transduction of spinal cord and brain compared to AAV9 (Ref.[7] and Supplementary Fig. S3). In contrast, while AAV-F generally mediated a slightly higher transduction efficiency in NHP spinal cord, there was little observed difference between the two capsids in the brain. In fact, widespread, yet, diffuse transduction of brain with both vectors were observed, similar to prior studies.[6] While some brain samples for qPCR had detectable genomes, many did not. This apparent discrepancy with the brain transduction data is likely due to the very small tissue punch from the contract research organization (CRO) that performed the NHP study for the qPCR and low yields of genomic DNA (average of 21 ng/μL). If higher amounts of fresh frozen material were processed, we would likely have been able to detect vector genomes for all samples in the brain. These data collectively suggest that barriers that limit AAV9 biodistribution/transduction in mice are likely different in NHPs. Furthermore, they point to the unpredictability of transduction properties of a given capsid from mice to NHPs. There are notable examples of transduction properties of a particular capsid (*e.g.*, AAV-PHP.B) translating from mice to NHPs[10] and examples in which it does not.[19,20] Performing AAV capsid library selections directly in NHPs may allow for a higher probability of clinically useful gene transfer properties of candidate capsids.

Algorithm-based IA approaches are powerful tools enabling for the detection of differences beyond the limit of the human eye. However, some IA systems can become biased due to a limited number of training data, which may not account for tissue heterogeneity or variability in tissue quality observed in later samples. To address this issue, we implemented a cell-based IA system led by the pathologist to measure GFP expression across different neuronal subtypes. This allowed for the computer to capture all the intricate cell features (size, shape, staining characteristics, and spatial relationship) from each sample's training regions while keeping the decisions with the pathologist. These cell features were then used by the algorithm to identify motor neurons and interneurons in each sample. Using this cell-based approach allowed for the pathologist to apply their expertise to each sample while utilizing the power of the IA system to generate precise and reproducible quantitative data. To our knowledge, this is the first study to use an automated IA approach to measure GFP expression of multiple neuronal types in the spinal cord. Demonstrated here is an unbiased, reliable, and accurate way to evaluate the transduction efficiency across AAV vectors. This is the first study to attempt to distinguish and quantify AAV-mediated transgene expression in both motor and interneurons in NHPs, although interneuron transduction by AAV9 was reported in mice.[21] This was facilitated using IA of phenotypic differences between the two cell types. This analysis provided interesting insights in the transduction profile between AAV-F and AAV9. For instance, in the thoracic region, AAV-F transduced a mean of 29.3% interneurons compared to 16.1% for AAV9. One other potentially important finding was the trend toward lower transduction efficiency (percentage) of DRG neurons with AAV-F compared to AAV9, although there was a very slight increase in mean stain intensity with AAV-F. Doses of AAV required to achieve efficient neuronal transduction in spinal cord can result in toxicity due to transgene overexpression in DRG.[14] Since AAV-F mediates transduction efficiency on par or higher than AAV9 in the spinal cord, and lower percentage of DRG transduction, the combination of this capsid with posttranscriptional reduction in transgene expression using microRNA seed sequences,[22] may help mitigate this toxicity. Along the same lines, we observed, on average, lower levels of AAV genomes with AAV-F compared to AAV9 in liver (Fig. 7b). Analysis of GFP expression by immunofluorescence imaging revealed all AAV-F injected NHP (regardless of sex) to have low percentages of GFP positive cells (Supplementary Fig. S9). In stark contrast, one male NHP injected with AAV9 had very high percentages of transduce hepato-

cytes, while the female NHP injected with AAV9 had almost no transduction. While it is firmly established that AAV vectors transduce murine liver higher in males than females,[23] it is less well-studied in NHPs, although there are some data which suggest that this may occur in the latter species as well.[24] Determining whether the high levels of transduction of AAV9 in male NHPs, and low transduction with AAV-F is reproducible, or a result of another factor will be of interest in future studies.

We also evaluated whether intrathecally injected AAV-F and AAV9 could transduce peripheral sciatic nerves. Transduction of peripheral nerve cells, including Schwann cells, would have utility to treat a variety of diseases ranging from schwannomas, and myelin disorders.[25] However, studies have been limited to rodents and cultured cells.[25,26] We made the interesting observation that AAV-F has the ability to transduce the sciatic nerve. While transduction appeared sparse, this was not observed with AAV9. Furthermore, the dose we used in the study was low, and injecting a 10-fold higher dose would be expected to improve transduction of the sciatic nerve.

Overall, our data performed an initial first look at AAV-F transgene expression performance after intrathecal delivery in NHPs. During the three week in-life study, intrathecal delivery of the AAV-F capsid was well tolerated. Although the number of animals was small in this exploratory study, the modest enhancement of transduction of motor neurons and interneurons with AAV-F as well as transduction of peripheral nerve Schwann cells is promising and warrants future dose ranging studies in larger groups of NHPs.

AUTHORS' CONTRIBUTIONS

C.A.M. and K.S.H. conceived of the study, designed experiments, performed experiments, analyzed data, and drafted and edited the article. Y.G. and A.B. performed experiments, analyzed data, and helped draft the article. J.C.M.K., K.H., J.N., C.N., and M.C. performed experiments. F.E., K.M.S., A.S.-R., and D.B.W. designed experiments, analyzed data, and edited the article.

ACKNOWLEDGMENTS

We thank Dr. Jessica Chichester of the University of Pennsylvania Human Immunology Core for performing the AAV9 neutralization assays.

AUTHOR DISCLOSURE

C.A.M. has a financial interest in Sphere Gene Therapeutics, Inc., Chameleon Biosciences, Inc., and Claritas Bio, Inc., companies developing gene therapy platforms. C.A.M.'s interests were reviewed and are managed by MGH and Mass General Brigham in accordance with their conflict of interest policies. C.A.M. and K.S.H. have a filed patent application surrounding the AAV-F capsid, and agreements between MGH and biotechnology companies have resulted in monetary payments around licensing agreements.

FUNDING INFORMATION

This work was supported by NIH grant DC017117 (to C.A.M.) and a sponsored research agreement (SRA) with SwanBio Therapeutics.

SUPPLEMENTARY MATERIAL

Supplementary Figure S1
Supplementary Figure S2
Supplementary Figure S3
Supplementary Figure S4
Supplementary Figure S5
Supplementary Figure S6
Supplementary Figure S7
Supplementary Figure S8
Supplementary Figure S9
Supplementary Figure S10
Supplementary Figure S11

REFERENCES

1. Keeler AM, Flotte TR. Recombinant adeno-associated virus gene therapy in light of Luxturna (and Zolgensma and Glybera): where are we, and how did we get here? Annu Rev Virol 2019;6:601–621.
2. Hinderer C, Katz N, Buza EL, et al. Severe toxicity in nonhuman primates and piglets following high-dose intravenous administration of an adeno-associated virus vector expressing human SMN. Hum Gene Ther 2018;29:285–298.
3. Morales L, Gambhir Y, Bennett J, et al. Broader implications of progressive liver dysfunction and lethal sepsis in two boys following systemic high-dose AAV. Mol Ther 2020;28:1753–1755.
4. Scallan CD, Jiang H, Liu T, et al. Human immunoglobulin inhibits liver transduction by AAV vectors at low AAV2 neutralizing titers in SCID mice. Blood 2006;107:1810–1817.
5. Manno CS, Pierce GF, Arruda VR, et al. Successful transduction of liver in hemophilia by AAV-Factor IX and limitations imposed by the host immune response. Nat Med 2006;12:342–347.
6. Gray SJ, Nagabhushan Kalburgi S, McCown TJ, et al. Global CNS gene delivery and evasion of anti-AAV-neutralizing antibodies by intrathecal AAV administration in non-human primates. Gene Ther 2013;20:450–459.
7. Hanlon KS, Meltzer JC, Buzhdygan T, et al. Selection of an efficient AAV vector for robust CNS transgene expression. Mol Ther Methods Clin Dev 2019;15:320–332.
8. Silva MA, Ryall KA, Wilm C, et al. PD-L1 immunostaining scoring for non-small cell lung cancer based on immunosurveillance parameters. PLoS One 2018;13:e0196464.
9. Echle A, Rindtorff NT, Brinker TJ, et al. Deep learning in cancer pathology: a new generation of clinical biomarkers. Br J Cancer 2021;124:686–696.
10. Gyorgy B, Meijer EJ, Ivanchenko MV, et al. Gene transfer with AAV9-PHP.B rescues hearing in a

mouse model of usher syndrome 3A and transduces hair cells in a non-human primate. Mol Ther Methods Clin Dev 2019;13:1–13.

11. Maguire CA, Balaj L, Sivaraman S, et al. Microvesicle-associated AAV vector as a novel gene delivery system. Mol Ther 2012;20:960–971.

12. Aeffner F, Martin NT, Peljto M, et al. Quantitative assessment of pancreatic cancer precursor lesions in IHC-stained tissue with a tissue image analysis platform. Lab Invest 2016;96:1327–1336.

13. Worner TP, Bennett A, Habka S, et al. Adeno-associated virus capsid assembly is divergent and stochastic. Nat Commun 2021;12:1642.

14. Hordeaux J, Buza EL, Dyer C, et al. Adeno-associated virus-induced dorsal root ganglion pathology. Hum Gene Ther 2020;31:808–818.

15. Meyer K, Ferraiuolo L, Schmelzer L, et al. Improving single injection CSF delivery of AAV9-mediated gene therapy for SMA: a dose-response study in mice and nonhuman primates. Mol Ther 2015;23:477–487.

16. Bey K, Deniaud J, Dubreil L, et al. Intra-CSF AAV9 and AAVrh10 administration in nonhuman primates: promising routes and vectors for which neurological diseases? Mol Ther Methods Clin Dev 2020;17:771–784.

17. Thomas CE, Storm TA, Huang Z, et al. Rapid uncoating of vector genomes is the key to efficient liver transduction with pseudotyped adeno-associated virus vectors. J Virol 2004;78:3110–3122.

18. Castle MJ, Cheng Y, Asokan A, et al. Physical positioning markedly enhances brain transduction after intrathecal AAV9 infusion. Sci Adv 2018;4:eaau9859.

19. Hordeaux J, Wang Q, Katz N, et al. The neurotropic properties of AAV-PHP.B are limited to C57BL/6J mice. Mol Ther 2018;26:664–668.

20. Hordeaux J, Yuan Y, Clark PM, et al. The GPI-linked protein LY6A drives AAV-PHP.B transport across the blood-brain barrier. Mol Ther 2019;27:912–921.

21. Lukashchuk V, Lewis KE, Coldicott I, et al. AAV9-mediated central nervous system-targeted gene delivery via cisterna magna route in mice. Mol Ther Methods Clin Dev 2016;3:15055.

22. Hordeaux J, Buza EL, Jeffrey B, et al. MicroRNA-mediated inhibition of transgene expression reduces dorsal root ganglion toxicity by AAV vectors in primates. Sci Transl Med 2020;12:eaba9188.

23. Davidoff AM, Ng CY, Zhou J, et al. Sex significantly influences transduction of murine liver by recombinant adeno-associated viral vectors through an androgen-dependent pathway. Blood 2003;102:480–488.

24. Gao G, Lu Y, Calcedo R, et al. Biology of AAV serotype vectors in liver-directed gene transfer to nonhuman primates. Mol Ther 2006;13:77–87.

25. O'Carroll SJ, Cook WH, Young D. AAV targeting of glial cell types in the central and peripheral nervous system and relevance to human gene therapy. Front Mol Neurosci 2020;13:618020.

26. Homs J, Ariza L, Pages G, et al. Schwann cell targeting via intrasciatic injection of AAV8 as gene therapy strategy for peripheral nerve regeneration. Gene Ther 2011;18:622–630.

Received for publication March 22, 2021;
accepted after revision June 5, 2021.

Published online: June 15, 2021.